AIMS Energy, 4(5): 658-674.
DOI: 10.3934/energy.2016.5.658
Received: 24 May 2016
Accepted: 10 August 2016
Published: 18 August 2016

http://www.aimspress.com/journal/energy

Research article

Design of a parallel-LC-compensated on-board charger for universal inductive charging in electric vehicles

Nan Liu* and Thomas G. Habetler

School of Electrical and Computer Engineering, Georgia Institute of Technology, Atlanta, GA 30332-0250, USA.

*** Correspondence:** Email: nliu37@gatech.edu; Tel: +770-826-7159.

Abstract: This paper proposes an on-board charger with a parallel-connected LC circuit which works in coordination with the previously-proposed universal charger to achieve "real" universal inductive charging. For accurately tracking the optimal frequency and achieving soft switching of the primary charger, an additional inductor is connected in series with the P-connected resonant tank to form an "LCL" topology. Based on the voltage gain of the proposed resonant topology, a step-down DC-DC converter is used to generate standard charging voltage and current to EV batteries. The detailed design method of the LCL circuit and DC-DC converter is provided. Theoretical analysis demonstrates that the proposed LCL-compensated secondary resonant circuit has a stable output voltage vs varied magnetic coupling and load. Compared with series-compensated LC circuits, the proposed topology has two main advantages: a smaller range of the varied optimal AC frequency vs magnetic couplings and a much lower voltage stress on the resonant capacitance. Experiments based on a prototype of inductive charging system prove that the proposed on-board charger has high DC-DC efficiency, a smaller range of AC frequency, and a universally-achieved stable output.

Keywords: DC-DC converter; electric vehicle; on-board charger; resonant circuit; universal inductive charger

List of Symbols

L_1, L_2	self-inductance of transmitting coil (primary inductance) and self-inductance of receiving coil (secondary inductance)
C_1, C_2	primary resonant capacitance and secondary resonant capacitance
M	mutual inductance between transmitting and receiving coils

L_{S2}	additional inductor connected to parallel-connected LC circuit in the LCL structure of on-board charger
k	coupling coefficient between transmitting and receiving coils
V_{in}, V_{out}	input voltage and output voltage of resonant circuits
I_1, I_2	currents in transmitting and receiving coils
V_o	charging voltage on EV batteries
R_{load}	equivalent resistance at the output of resonant circuit
R_{eq}	equivalent resistance for power consumption of EV batteries
G	voltage gain in DC characteristics of resonant circuits
f_0	resonant frequency of a resonant circuit
f_1	fixed-gain frequency of resonant circuits
D	duty cycle of DC-DC converter

1. Introduction

Inductive power transfer (IPT) technology is a promising method for conveniently, safely, and efficiently charging electric vehicle (EV) batteries [1-3]. Different from traditional conductive charging, the basic principle of inductive charging is to transfer AC power from a primary charger to one or multiple receivers through magnetic coupling between the charging interfaces on the two sides [4]. IPT has many advantages over traditional plug-in charging such as galvanic isolation and better stability in harsh environments [5,6]. Besides the traditional applications in home garage or public parking lots, inductive charging has more applications such as roadway electrification. The basic structure of an inductive charging system consists of two parts: a primary charger which generates AC power and a receiver which receives power wirelessly and provides standard charging voltage and current to EV batteries. AC power is transferred through the magnetic coupling between the two interfaces. Each interface mainly consists of a coil carrying AC current and a ferrite structure on the back of the coil forcing magnetic flux flow in loop. Because of low coupling, the AC power should be carried by an LC resonant circuit in the primary charger and an LC resonant circuit on EV. The charging interfaces work as the inductors in LC circuits. Therefore, the electrical characteristics of the resonant circuits directly determine the system performance [7].

Despite the fact that inductive charging is more convenient and aesthetic, some technical problems still limit practical applications of IPT. First, the magnetic coupling effect between the two charging pads varies when the tire pressure or the horizontal position of the charged EV changes. The varied magnetic coupling changes the electrical performance and leads to system instability. Secondly, many EV models are currently on the market and more will be released in the future. The growing market needs a universal charger which is suitable for charging various EV models with varied magnetic coupling. Universal inductive charging will have broad applications, especially in public charging areas. To solve the problems of varied magnetic coupling and multiple EV models, a universal inductive charger (UIC) which is installed on the ground (primary side) is proposed in [1]. The UIC generates a stable charging voltage even when the magnetic coupling is changed by the varied air gap or horizontal misalignment. Moreover, the UIC aims at charging a receiver with either series- (S-) or parallel-connected (P-connected) LC circuit. By feasible designs, S- and P-connected LC circuits are good enough for most applications, although there are a lot of more complicate

topologies. By common sense, a simple LC circuit does not need complicate system control. Also, more L's or C's commonly mean more complex control and more power loss. Therefore, the proposed universal charging mainly considers the two basic LC topologies on loads. In [8], an on-board charger with an S-connected LC is proposed to work in coordination with the UIC. However, an on-board charger with an S-connected LC circuit has disadvantages such as a large optimal-frequency range and high voltage stress on the resonant capacitor. This means S-connected LC circuit is limited in some applications. Moreover, the definition of the UIC requires a design scheme of on-board chargers containing P-connected LC circuit, besides S-connected LC circuit. Different from common designs applying P-connected LC circuit, the on-board charger proposed in this paper is specifically designed for universal inductive charging which employs an S-compensated primary LC circuit and a variable-frequency method [1]. The proposed designs of both sides can be used as a design method of universal EV inductive charging system.

The main aim of this paper is to design an on-board charger with a P-connected LC circuit which works in coordination with the UIC and realizes universal inductive charging. The design contains three main elements: the secondary LC resonant circuit, the design and control of the DC-DC converter, and the design of the receiving pad (coil). First, a better design of the secondary LC circuit generates a stable output voltage vs varied coupling and load, meaning that the input of the on-board converter is stable. This paper applies a P-connected secondary LC circuit in universal inductive charging. Previous research has analyzed S-connected LC's, P-connected LC's, and more complicate designs such as LCL and LCC circuits [8-14]. S-connected and P-connected LC circuits are two basic topologies. By circuit analysis, an S-connected LC circuit is easier to tune and performs better in harmonics reduction, while a P-connected LC circuit acts as a current source which can be more suitable for charging batteries [1,9]. Some other topologies are also proposed for some specific applications. For example, in [9], an on-board charger (pickup) with a series-parallel-tuned LCL topology combines the electrical characteristics of S-connected and P-connected LC circuits and realizes a unity power factor of the load. However, the on-board charger in [9] cannot deal with variances in magnetic coupling. The operation and efficiency of the primary charger is lower than traditional S-connected LC circuit, because the primary current can be very high when the magnetic coupling is low. In [15], the on-board charger applies a dynamically detuned LC resonant circuit, which is changed by turning on and off a semiconductor switching device. A dynamically-detuned LC circuit is used to stabilize the output voltage vs load and magnetic coupling. However, the added switch needs more complicate control and increases cost. The proposed detuned method over varied magnetic coupling is also very limited. In fact, without coordination between the primary charger and the on-board charger, the system always has some practical problems in universal charging. Secondly, the design and modulation of the AC-DC converter are based on the DC characteristics of LC resonant circuits and the control strategy of the primary charger. Because the topology of an LC resonant circuit is not changed in common designs, the on-board converter is the only adjustable part of the on-board charger. The input of the converter is the output of the resonant circuits and the output of the converter is the charging voltage and current. The converter must be controlled according to the charging profiles of EV batteries. For easy and stable control of the DC-DC converter, a constant input voltage of the converter or the output voltage of the resonant circuits is necessary. Common DC-DC converters, such as fly-back converters or resonant converters, are applied by previous research [9,16-18]. Power factor correction is commonly employed by the on-board converter. In the same example of [9], a boost converter is used as the on-board DC-DC

converter to control the charging voltage and current while modulating the overall impedance of the load side. According to the DC characteristics of SP-connected LC circuits and the fixed-gain point of the UIC, a step-down converter is used for DC-DC conversion in this paper [1]. Thirdly, the plane-core structure is the most commonly used structure for charging interfaces, also known as "pad" [18]. There are two types of charging pads: polarized and non-polarized pads [5,19-22]. The non-polarized pad contains a single coil and generates perpendicular magnetic flux between the transmitter and the receiver. The polarized pad has two coils which are reversely polarized and the flux flows in the loop formed by two transmitting coils and two receiver coils. Research in [1] and [8] demonstrate that the non-polarized pad is more efficient in practical applications where the size of charging pads is limited by EV chassis. The non-polarized pad is also widely employed in most of current research on inductive charging. Therefore, the proposed design employs non-polarized receiving pad. Other design details of the receiving pad are designed based on the required characteristics of the primary and secondary sides such as voltage gain and power levels.

In this paper, an on-board charger with a P-connected LC resonant circuit is proposed. Considering the on-board chargers with S-connected LC circuit on EV, the proposed design with a P-connected LC circuit is the one last piece of the "universal charging". The currently-existing problems of on-board chargers with P-connected LC circuit are solved. To improve the accuracy of frequency tracking and maintain soft-switching of the primary DC-AC inverter, an additional inductor is series connected to the P-connected LC circuit. A step-down converter is chosen as the DC-DC converter according to the electrical characteristics of the resonant circuits. Based on the proposed design, the advantages of the proposed on-board charger are analyzed, including a much smaller range of optimal frequencies and lower voltage stress on the resonant capacitors. Experimental results validate that the proposed design has a stable output voltage vs varied coupling and load, high efficiency, and a small range of optimal AC frequency.

2. Materials and Methods

A specific design standard of on-board chargers with P-connected LC circuit is proposed in this paper, based on the scheme of "universal inductive charging". A universal inductive charger (UIC) is proposed to adaptively provide stable charging voltage to various EV models even with the influence of various receiving coils and varied magnetic coupling [1]. By previous analysis, the proposed UIC applies variable-frequency control: the UIC gradually increases the AC frequency from the resonant frequency to higher values by a fixed step and measures the overall load-phase angle. The optimal AC frequency is tracked when the load-phase angle of the resonant circuits reaches the zero-crossing point. The variable-frequency control works well for both S-connected and P-connected secondary LC circuits. In [2], an on-board charger with an S-connected secondary LC is proposed to work in coordination with the UIC. However, the P-connected LC circuit has some advantages over S-connected LC circuit such as a smaller range of optimal AC frequency. On the other hand, an applicable standard of designing an on-board charger with a P-connected LC circuit is necessary to achieve the proposed universal inductive charging. With the design of a parallel-LC-compensated on-board charger, the design of the whole system can be used as a feasible method for EV inductive charging.

2.1. Existing problems of SP LC circuits

The equivalent topology of the on-board charger with a P-connected LC circuit is shown in Figure 1. The simulated DC characteristics of a SP-connected LC circuit, including the voltage gain and the load-phase angle vs the AC frequency, are shown in Figure 2. In Figure 2, f_0 is the resonant frequency, and the frequency f_1 is the optimal AC frequency for the UIC to track. If the AC frequency is f_1, the voltage gain is constant vs the equivalent load resistance R_{load}. Based on the DC characteristics, there are challenges of applying a P-connected secondary LC circuit. First, the voltage control of the universal inductive charger may not be stable enough, because the voltage gain varies sensitively vs the AC frequency. According to the curves of the voltage gain, a tiny error of AC frequency from the fixed-gain point leads to a distinct difference from the fixed voltage gain when R_{load} is small. Another challenge is the inaccurate frequency control of the UIC. According to theoretical calculations, the load-phase angle is slightly lower than 0 when the frequency is at the fixed-gain point. In other words, the zero-crossing point of the load-phase angle is higher than the fixed-gain point. Therefore, the voltage gain cannot be maintained stable. Moreover, the difference between the fixed-gain point and zero-crossing point of the load-phase angle increases when the load resistance R_{load} increases. The error is exacerbated in practical applications, because of parasitic resistance on coils. As a result, with a SP topology, the fixed-gain point cannot be accurately tracked. A stable voltage gain vs R_{load} is difficult to be maintained. The existing problems of SP-connected LC circuits should be solved before the universal inductive charging can be achieved.

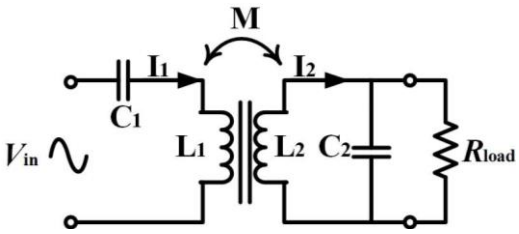

Figure 1. The equivalent topology of the inductive charging system with a P-connected LC circuit.

2.2. Application of step-down DC-DC converter

Based on the results in Figure 2, if the load contains a P-connected LC circuit and the AC frequency is at the fixed-gain point, the voltage gain keeps constant within varied load conditions, as

$$G = \left| V_{out} / V_{in} \right| = L_2 / M \ . \tag{1}$$

According to the design of the charging interface in [8], a larger receiving pad leads to better coupling and a higher power-transfer capability. A reasonable design of the receiving pad is of the similar size of the transmitting pad, for the tightest coupling and the highest power-transfer capability when the size of the receiving pad is limited [8]. If the coupling coefficient ranges from 1/10 to 1/5, the fixed voltage gain ranges from 10 to 5, which is much higher for charging EV batteries in the whole range of load. Thus, the on-board converter should convert the high voltage to a lower value. The topology of the on-board charger is shown in Figure 3. A diode rectifier connected to the output of the secondary LC circuit achieves the initial AC-DC conversion. At the

back end of the rectifier, a DC-DC converter with PFC is employed to provide standard charging voltage V_o and current I_o to the battery system which is commonly formed by battery arrays and a battery management system (BMS) [22,23].

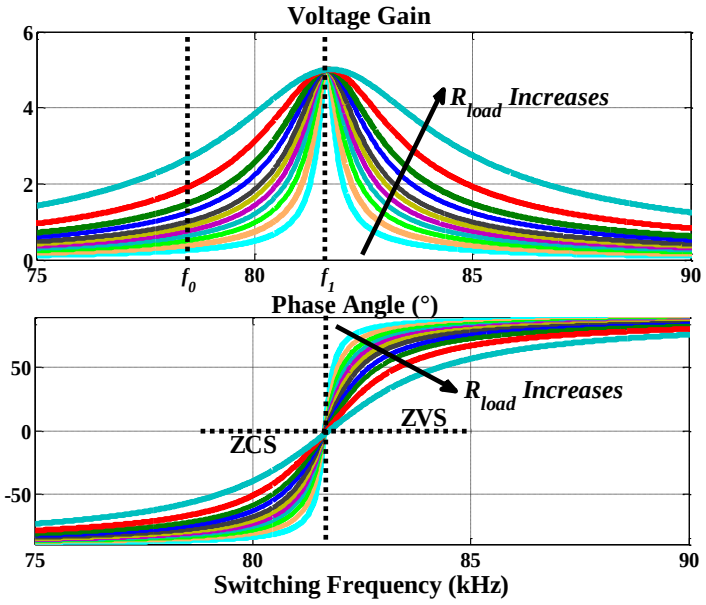

Figure 2. The DC characteristics: the voltage gain and the load-phase angle vs the AC frequency in the SP-connected LC circuits, when the primary LC includes L_1 = 199.5 μH and C_1 = 20.87 nF, the secondary LC includes L_2 = 200.8 μH and C_2 = 20.73 nF, M = 40 μH (k = 0.2), and R_{load} = 10, 15, 20, 25, 30, 35, 40, 50, 60, 80, 120 Ω [1].

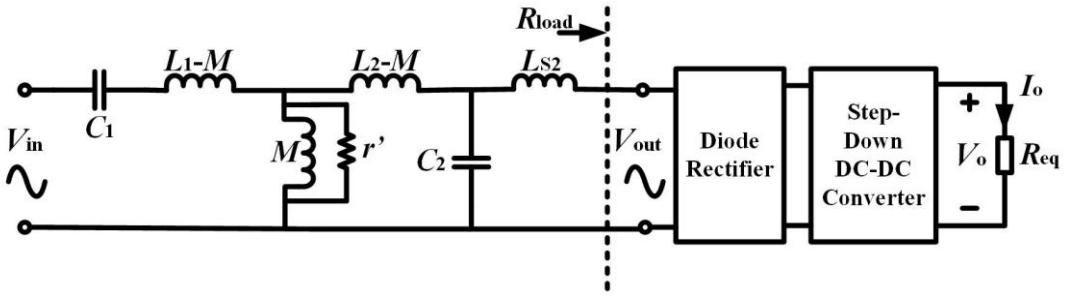

Figure 3. The equivalent topology of the inductive charging system with the on-board converter containing a P-connected LC circuit and an additional inductor L_{S2}.

There are papers and reports published in the area of EV battery charging [16,18,24-26]. For commonly-used lithium-ion batteries in EV, the charging process has two main steps: constant-current and constant-voltage charging. To charge almost-empty EV battery, the charging current is kept constant and the voltage increases rapidly at the beginning of the first step. Then the increasing speed of the charging voltage becomes slower. Before the second step begins, the battery voltage climbs quickly again when the battery is almost fully charged. At that moment, the second-step charging is operated: the on-board charger senses the variances of the battery voltage

and applies a constant voltage until charging process ends (current low enough). If the charging process starts with battery that is not fully drained, the charging voltage and current should be controlled according to the specific charging profile of EV battery. Thus the charger should detect the battery status before a charging process begins. The back-end DC-DC converter can easily operate the two steps of charging if the input voltage is stable. Thus the output voltage of LC circuit should be adaptively kept stable vs k or load. The DC characteristics of resonant circuits: the fixed-gain point vs varied load conditions is mainly analyzed in this paper.

In practical applications, manufacturers should design the receiving coil (or the estimated range of L_2/M) and the DC-DC converter based on possible V_{out} of resonant circuits and the range of standard V_{o} of EV batteries. If V_{in} = 200 Vrms, the output voltage of diode bridge typically ranges from 1000 V to 2000 V, according to Equation (1). Based on a typical example - the EV battery pack of Nissan Leaf, the standard charging voltage starts from 300 V to 420 V during the charging process (from the heaviest to the lightest load condition) [11,27]. Therefore, the voltage gain of the step-down converter applied ranges from 0.42 to 0.15:

$$V_{o,converter} / V_{in,converter} = D .$$

If the input of the DC-DC converter is very stable vs varied coupling and load, the output can be easily controlled during the charging process, including the output-voltage control and over-voltage protection.

A reasonable equivalent model of batteries is necessary in analysis of output of resonant circuits vs load (active power). In fact, battery pack in EV's is commonly a high inertial load. From the view of DC charging ports, a resistive load can be used to represent the power consumption of batteries in steady state. Most of battery chargers also have the function of PFC and resistive impedance is reflected to resonant circuits. Therefore a varied resistance can be used to analyze the varied power consumptions of lead-acid or lithium-ion batteries during a charging cycle [3,11,12,28-30]. Power consumption of EV batteries is simply represented by varied R_{eq} in this paper. R_{load} is the equivalent resistance reflected from the load to the output of the secondary LC circuit. Theoretically, if the step-down converter is a BUCK converter, the equivalent resistance looking from the output of the secondary LC circuit can be approximately calculated by

$$R_{load} \approx \left(1/D^2\right) R_{eq} \cdot p_{DC \to AC}, \tag{2}$$

where $p_{DC \to AC}$ is the parameter used for converting the resistance R_{eq} at the DC output DC-DC converter to the resistance R_{load} at the AC output of the secondary LC circuit.

$$p_{DC \to AC} = 8 / \pi^2 ,$$

when the first-stage AC-DC converter is of a full-bridge structure.

The application of a step-down converter has another advantage: more stable output vs frequency. The equivalent resistance R_{load} reflected to the output of the secondary resonant circuit is larger than the equivalent resistance R_{eq} of the batteries. A larger value of R_{load} means more stable output voltage V_{out} of the secondary LC circuit, because the voltage gain is more sensitive to frequency variances when R_{load} is smaller, according to the voltage-gain curves Figure 2. This advantage helps generate a stable voltage output when the AC frequency has an error from the

theoretical value. When the coupling coefficient k = 0.20, the voltage gain at the fixed-gain point is G = 5. A buck converter is used to charge EV batteries with the nominal voltage 400 V. The duty cycle of the buck converter will be around 0.4. According to the charging profile of battery of Nissan Leaf, the nominal charging voltage varies from 300 to 420 V and the nominal charging current varies from 10 to 1 A [11,27]. Thus, R_{eq} = 40~300 Ω is used to represent charging power in most of common load conditions. By Equation (2), R_{load} = 200~1520 Ω. The curves of DC characteristics vs AC frequency are shown in Figure 4(a).

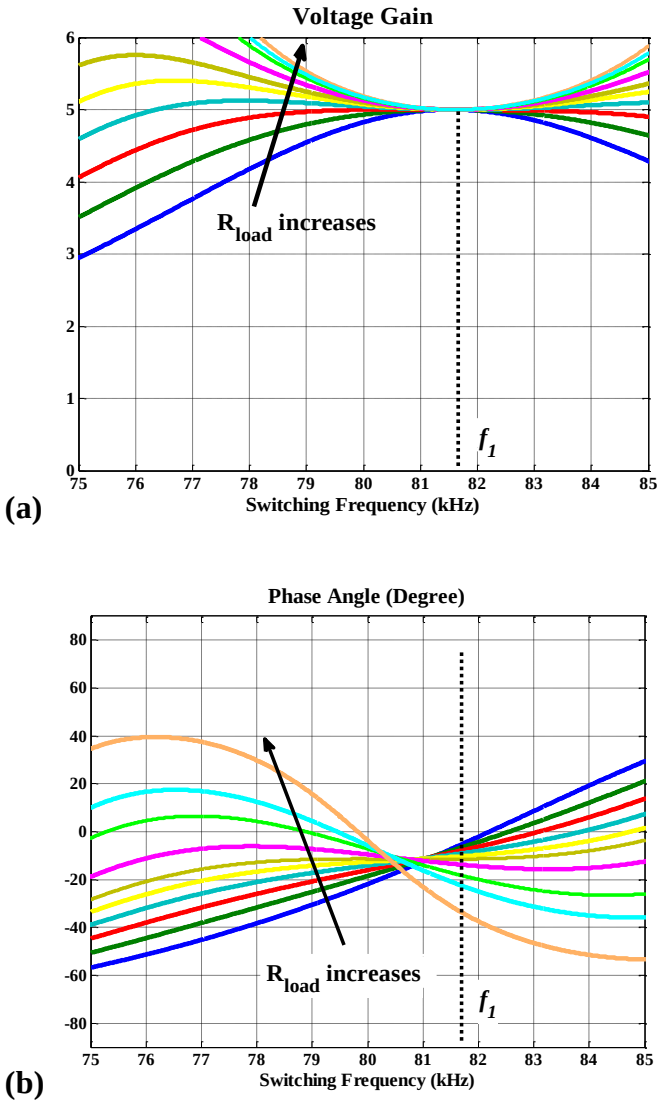

Figure 4. The curves of (a) the voltage gain and (b) the load phase angle vs the AC frequency in the SP-connected LC. Topology parameters: L_1 = 199.5 μH, C_1 = 20.87 nF, L_2 = 200.8 μH, C_2 = 20.73 nF, M = 40 μH (k = 0.2), and R_{load} = 200, 250, 300, 400, 500, 600, 800, 1000, 1200, 1600 Ω.

In Figure 4(a), the voltage-gain curves vary from a 'bulge' to a 'hollow' when the equivalent load resistance R_{load} increases. The variation trend of the voltage gain vs AC frequency is much more stable than the curves in Figure 2. However, the zero-crossing points of the load-phase-angle curves

are shifted from the fixed-gain point f_1 to other points. As R_{load} increases, the zero-crossing point of load-phase angle moved to be higher and then be lower than f_1. When R_{load} is large than 600 Ω, the load-phase-angle curves vs AC frequency vary in different trend and the zero-crossing point becomes lower than f_1. ZVS cannot be maintained when the load becomes light. Moreover, there is a range of R_{load} which does not own zero-crossing point of the load-phase angle higher than f_1. Therefore, the fixed-gain point f_1 cannot be accurately tracked in the whole range of R_{load}. With an inaccurate frequency, the load-phase angle may be always lower than zero, meaning ZVS of primary DC-AC inverter can never be achieved.

2.3. Additional inductor on P-connected LC topology

By previous analysis, the zero-crossing point of a load-phase-angle curve varies from the fixed-gain point f_1 when the load R_{load} becomes larger. Thus, the frequency at the fixed-gain point cannot be accurately tracked when R_{load} is large enough. Moreover, the load-phase angle at the fixed-gain point is lower than 0, meaning that ZVS of the primary DC-AC inverter cannot be adaptively realized. To accurately track f_1, an additional inductor is connected in series with the secondary LC resonant tank (similar as an "LCL" circuit), as L_{S2} in Figure 3:

$$L_{S2} = \eta_2 L_2 .$$

Based on the primary LC circuit in Figure 2, the DC characteristics of the system with a secondary "LCL" circuit are calculated, as shown in Figure 5. In Figure 5(b), a reasonable L_{S2} = 8 μH generates the zero-crossing point of the load-phase angle locating at the fixed-gain point f_1. Because the tracked frequency is usually higher than f_1, the load-impedance angle is higher than 0 in the heavy and medium load conditions: R_{load} = 200~600 Ω. Obviously, ZVS operation of the primary DC-AC inverter is realized in a wide range of load conditions. If the mutual inductance M decreases to be the lowest value: 20 μH (k = 0.1), the DC characteristics are shown in Figure 6. In Figure 6, the fixed-gain point moves towards the resonant frequency when M decreases. When the AC frequency is set to be the fixed-gain point, the load-phase angle is always higher than 0, leading to durative ZVS of the DC-AC inverter. In summary, the fixed-gain point can be tracked in the whole range of k and ZVS is also universally achieved.

The value of L_{S2} is determined when all load-phase-angle curves with the highest M have the same zero-crossing point locating at the fixed-gain point. After choosing L_{S2}, ZVS operation of the DC-AC inverter can be maintained in various load conditions, when M is equal to or smaller than the highest value. When R_{load} becomes larger, the zero-crossing point of the load-phase angle is moved to be lower. This means that the accuracy of frequency tracking is influenced when R_{load} is larger at the beginning of a charging cycle. However, according to the currently under-research standard SAE J2954, the limitation of AC frequency wireless charging of EVs ranges from 81.39 to 90 kHz. The frequency should be the lowest value 81.39 kHz if the acquired optimal frequency by R_{load} is lower than 81.39 kHz. In this condition, the range of the varied voltage gain during the charging cycle is very small, as shown in Figure 6. More importantly, ZVS of the DC-AC inverter is maintained.

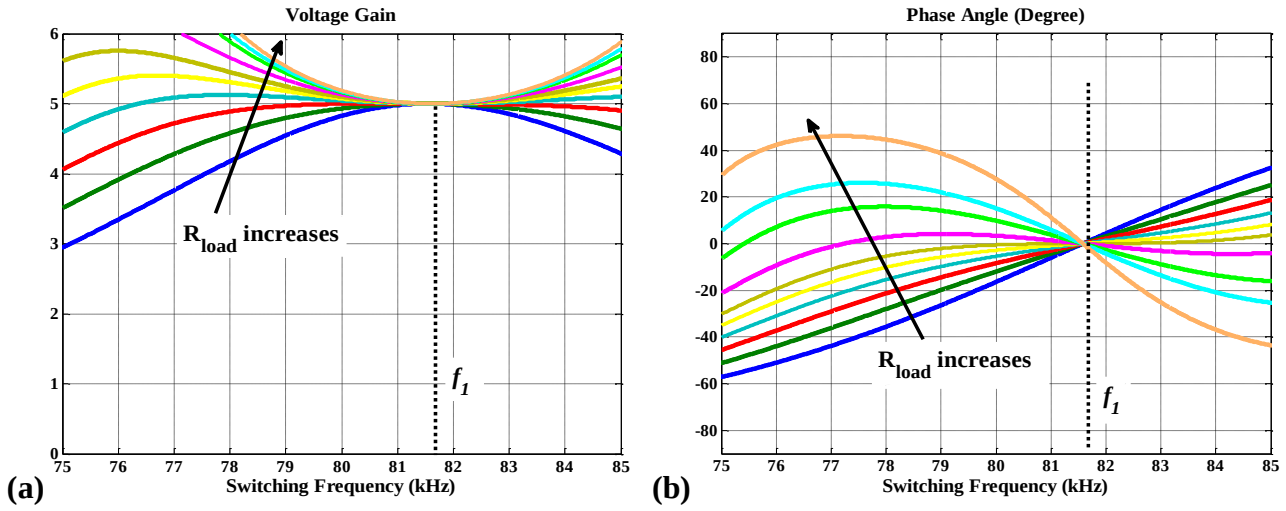

Figure 5. The curves of (a) the voltage gain and (b) the load-phase angle vs the AC frequency in the SP-connected LC with additional inductor L_{S2} = 8 μH. Topology parameters: L_1 = 199.5 μH, C_1 = 20.87 nF, L_2 = 200.8 μH, C_2 = 20.73 nF, M = 40 μH (k = 0.2), and R_{load} = 200, 250, 300, 400, 500, 600, 800, 1000, 1200, 1600 Ω.

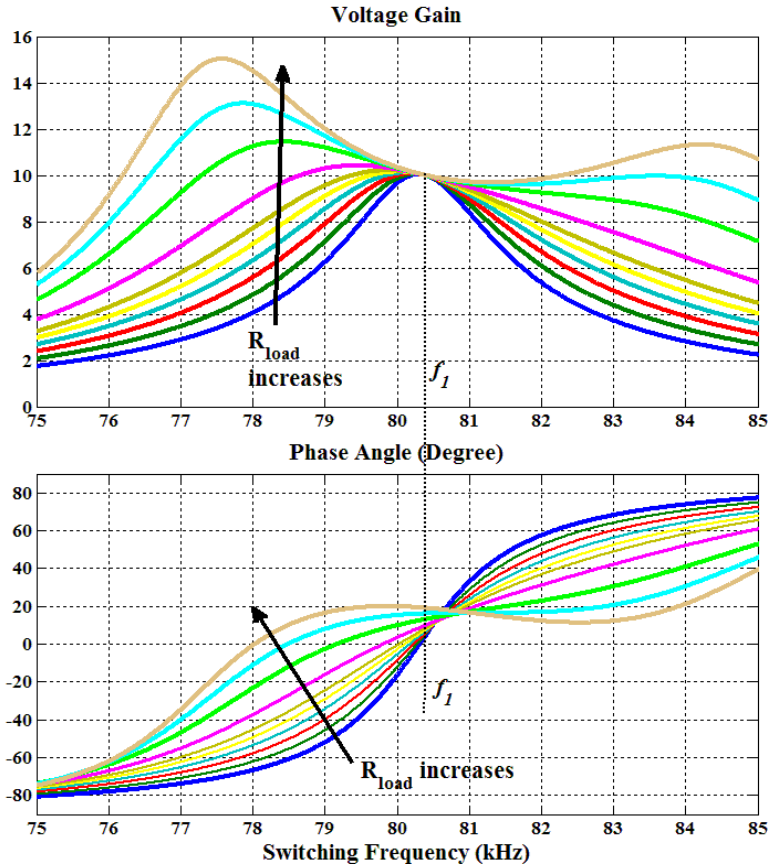

Figure 6. The curves of (a) the voltage gain and (b) the load-phase angle vs the AC frequency in the SP-connected LC with additional inductor L_{S2} = 8 μH.

2.4. Performance analysis of proposed charger

2.4.1. Smaller range of frequency variations during universal charging

Variable-frequency control is commonly applied in wireless charging of EV's. A better design has a smaller range of AC frequency for the full range of load conditions. Compared with the IPT system containing an S-connected secondary LC circuit, the system containing a P-connected secondary LC circuit has a much smaller frequency range of the fixed-gain point when the range of the magnetic coupling coefficients is fixed. By circuit analysis in [1], the fixed-gain point f_1 of the SS-connected LC circuits is

$$f_1 = \sqrt{\frac{\sqrt{L_2}}{C_1(L_1\sqrt{L_2} - M\sqrt{L_1})}} / 2\pi = \sqrt{\frac{1}{1-k}} \cdot f_0 . \tag{3}$$

When the secondary LC circuit is P-connected (SP-connected LC circuit), the frequency at the fixed-gain point f_1 is

$$f_1 = \sqrt{\frac{L_1}{C_2(L_1L_2 - M^2)}} / 2\pi = \sqrt{\frac{1}{1-k^2}} \cdot f_0 . \tag{4}$$

As a result, the range of the fixed-gain point f_1 with a P-connected LC circuit in load is much smaller than the range of f_1 with an S-connected LC circuit. For example, if k = 0.1~0.2, the range of f_1 with an S-connected secondary LC circuit is (1.054~1.118) • f_0 and the range of f_1 with a P-connected secondary LC circuit is (1.005~1.021) • f_0. When the resonant frequency of both LC circuits is f_0 = 80 kHz, the range of f_1 vs k with a P-connected secondary LC circuit is in 1.28 kHz, which is much smaller than the range of f_1 with an S-connected secondary LC: 5.12 kHz [1]. Moreover, when the coupling is guaranteed to be tight enough, for instance, k > 0.15, the variation of the voltage gain is very small (<3%) in a 1.28-kHz frequency range. This means the charger can apply a constant-frequency control and a stable voltage gain can still be maintained.

2.4.2. Low voltage stress on resonant capacitors

One problem of inductive charging for EVs is the high voltage stress on resonant capacitors. Because of the high AC frequency (>80 kHz) and high current (maximum 20 Arms), the highest voltage on the resonant capacitors can be higher than 2000 Vrms. The high voltage stress on resonant capacitors requires high voltage tolerance of the resonant capacitors in practical applications. Researchers commonly need to series connect multiple capacitors to reduce the voltage stress on each capacitor. However, the method of require a larger space and higher cost. P-connected secondary LC circuit has lower voltage stress on the resonant capacitor than the value of an S-connected secondary LC circuit.

To compare the voltage on capacitances in the SS-connected LC topology and the SP-connected LC topology, let the two LC topologies have the equal L_1's, L_2's, C_1's, C_2's, the identical range of load resistances, and the identical range of possible coupling coefficients. The voltage on C_2 in the SP-connected LC topology is equal to the output voltage of the secondary LC circuit, as

$$V_{C2,SP} = V_{out,SP} .$$

For the SS-connected LC topology, the voltage on C_2 is calculated by

$$V_{C2,SS} = \frac{V_{out,SS}}{R_{load,SS}} \cdot Z_{C2,SS} = \frac{V_{out,SS}}{R_{load,SS}} \cdot \frac{1}{(j\omega C_2)_{SS}} .$$

At the fixed gain point f_1, the ratio between the RMS output voltages of the two different topologies is

$$\frac{V_{out,SP}}{V_{out,SS}} = (\frac{L_2}{M} \cdot V_{in}) / (\sqrt{\frac{L_2}{L_1}} \cdot V_{in}) = \frac{1}{k} .$$

Therefore, the ratio between the RMS voltage on C_2 in two different topologies is

$$\frac{V_{C2,SP}}{V_{C2,SS}} = \frac{1}{k} \cdot \frac{R_{load,SS}}{Z_{C2}} = \frac{(1-D_{SS})^2 \cdot R_{eq} \cdot (8/\pi^2)}{k \cdot Z_{C2,SS}} , \quad (5)$$

where D_{SS} is the duty cycle of the on-board DC-DC converter in nominal condition. For an SP-connected topology, $V_{C2,SP}$ is of the maximum with the lowest k. The $V_{C2,SS}$ reaches the highest value when R_{eq} is the smallest. Based on the previous example, the fixed voltage gain of an SS-connected LC topology is nearly 1 and the theoretical D_{SS} = 0.5, when L_1 = L_2 for both LC topologies. If the AC frequency f_{sw} = 81 kHz and $R_{eq,min}$ = 40 Ω,

$$V_{C2,SP,max} / V_{C2,SS,max} = 0.6 .$$

Apparently, the highest voltage on C_2 in an SP-connected topology is lower than the value in an SS-connected topology. In practical applications, The ratio of $V_{C2,SP,max}/V_{C2,SS,max}$ is further reduced in an SP-connected LC topology because L_2 is typically smaller than L_1. For a SP-connected LC, a smaller L_2 ($<L_1$) leads to a reasonable input voltage of the DC-DC converter, according to the fixed voltage gain L_2/M in Equation (1). This helps avoid a too high output voltage of the SP-connected LC with a loose coupling effect, such as k = 0.1. For example, when L_2/L_1= 0.6 and k = 0.1~0.2, the fixed voltage gain is L_2/M = 7.746~3.873 < 10.

3. Results and Discussion

Based on the proposed design, a prototype of the on-board charger with a P-connected LC ("*LCL*" topology) circuit is built. The parameters of the load design are listed in Table 1. Note that the equivalent load resistances are used to represent power consumption of an on-board DC-DC converter (a step-down converter here) and batteries. The range of R_{load} in Table 1 is used as the equivalent resistance of batteries (R_{eq}) varying from 50 to 250 Ω, when the step-down ratio of the DC-DC converter is 0.5.

3.1. Stable output voltage

The normalized voltage gain of the resonant circuits vs R_{load} is shown in Figure 7, with three different air gaps (various coupling coefficients). When the load resistance R_{load} increases, the error between the theoretical and practical values is kept in a range of (−10~12%). This range is much

smaller than the range of the voltage gain with other frequencies, meaning that the output voltage of resonant circuit is stable in a charging cycle. One reason for variance of the voltage gain vs R_{load} is the error of the selected AC frequency: the AC frequency is not at the exact fixed-gain point. By theoretical results in Figure 5, if the AC frequency is close to the fixed-gain point, the voltage gain increases as the equivalent load resistance R_{load} increases. Another reason for variance of the voltage gain is from the voltage drop by parasitic components in the LC circuit, such as parasitic resistance of coils. The voltage drop of coil resistance is higher if R_{load} is smaller or the current is higher. Similar as the system with SS-connected LC circuits, the voltage gain varies in a larger range when air gap increases [8]. When the air gap increases, the influence on the voltage gain by inaccurately tracked frequency becomes more obvious, because the voltage drop on parasitic components in the primary side becomes higher.

Table 1. Parameters of receiving pad.

Parameters	Values
Dimensions of Transmitting Pad	Square Pad. Inner edge 28 cm, outer edge 40 cm. 8 Ferrite bars placed on back. Turn NO. 20 by 2 strands.
Dimensions of Receiving Pad	Square Pad. Inner edge 24 cm, outer edge 40 cm. 6 Ferrite bars placed on back. Turn NO. 15.
Coil Inductances	L_1 = 199.5 μH , L_2 = 135.5 μH
Resonant Capacitances	C_1 = 20.87 nF, C_2 = 29.21 nF
Additional Inductor L_{S2}	5.0 μH
Equivalent R_{load}	200, 250, 300, 350, 450, 550, 700, 1000 Ω

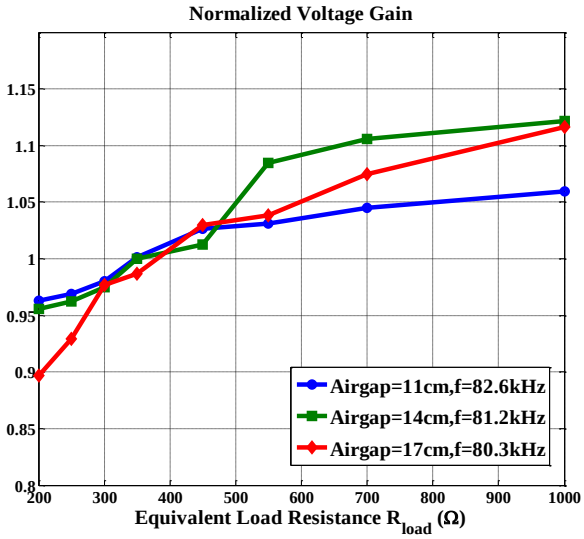

Figure 7. With three different air gaps, the measured voltage gain vs load resistance R_{load} when the UIC charges the proposed on-board charger with a P-connected secondary LC circuit.

3.2. High efficiency

The system efficiency (from the DC input of the primary inverter to the output of the diode rectifier) vs R_{load} is shown in Figure 8. The highest efficiency is higher than 94%. Obviously, the efficiency is reduced when the air gap increases. Different from SS-connected resonant circuit, the efficiency increases when load resistance increases [1]. The reason for the efficiency variance is from the equivalent model of an SP-connected structure, as a constant-current source. This is similar to the efficiency trend of a constant-current model, which has higher output power and efficiency when R_{load} becomes larger, although the proposed system realizes a constant-voltage output of the system.

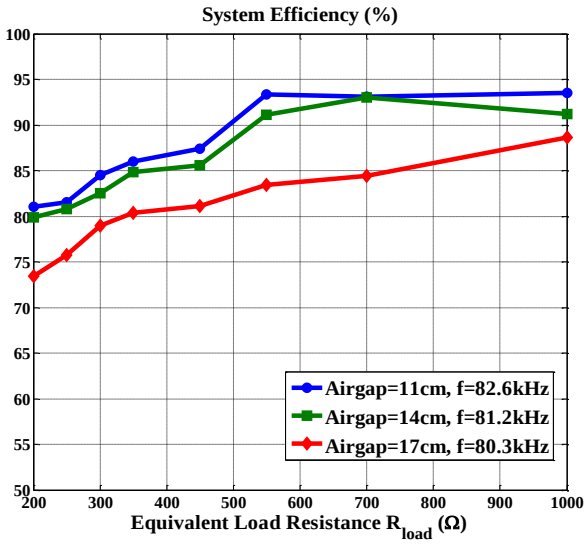

Figure 8. With three air gaps, the measured DC-DC efficiency vs load resistance R_{load} of an inductive charging system with a P-connected secondary LC circuit.

3.3. Small range of AC frequency

The selected optimal frequencies vs air gap demonstrate the smaller range of the optimal frequency vs varied magnetic coupling. As shown in the legend of Figure 7, the selected optimal AC frequency decreases when the air gap increases (magnetic coupling decreases). Compared with the previous on-board charger with an S-connected LC circuit which has a frequency ranging from 88.6 kHz to 83.7 kHz [1], the optimal AC frequency by this design ranges from 82.6 kHz to 80.3 kHz when the air gap changes from 11 cm to 17 cm. A smaller range of optimal frequency means more universal frequency control and better system stability.

For practical applications, the design scheme can also be universally applied in other cases which have different standard voltage and current. The analysis of the DC characteristics is the basis of the proposed design. For the secondary P-connected LC circuit in load, the values of L and C are very easy to determine according to the proposed voltage gain in Equation (1) and the standard resonant frequency. For the inductor L_{S2} series-connected to the P-connected LC circuit, the value is determined when the coupling is the highest. In summary, all resonant components are determined in just one case and do not need to consider the whole range of load or coupling.

4. Conclusion

This paper develops an on-board charger with a P-connected LC circuit which works in coordination with the UIC. The proposed on-board charger is one of the two main parts of the universal inductive charging system. Different from common on-board chargers applying a P-connected LC circuit, an additional inductor is connected in series with the P-connected resonant tank to form an "LCL" structure. The LCL topology leads to the equality of the fixed-gain point and the zero-crossing point of the load-phase-angle curves, meaning that the optimal AC frequency can be tracked and ZVS of UIC is achieved. According to the fixed voltage gain of the resonant circuits, a voltage-step-down DC-DC converter provides standard charging voltage and current to EV batteries. Better performance of the proposed design is theoretically analyzed. Hardware experiments are applied to demonstrate the advantages of the proposed design: better universality to varied load and magnetic coupling, high efficiency, more accurate frequency control, and a much smaller range of frequencies.

Conflict of interest

All authors declare no conflicts of interest in this paper.

References

1. Liu N, Habetler TG (2015) Design of a Universal Inductive Charger for Multiple Electric Vehicle Models. *IEEE T Power Electr* 30: 6378-6390.
2. Liu N, Habetler TG, A study of designing a universal inductive charger for Electric Vehicles. *Industrial Electronics Society, IECON 2013-39th Annual Conference of the IEEE*. IEEE, 2013: 4528-4533.
3. Yilmaz M, Krein PT (2013) Review of Battery Charger Topologies, Charging Power Levels, and Infrastructure for Plug-In Electric and Hybrid Vehicles. *IEEE T Power Electr* 28: 2151-2169.
4. Capasso C, Veneri O (2015) Experimental study of a DC charging station for full electric and plug in hybrid vehicles. *Appl Energ* 152: 131-142.
5. Zaheer A, Hao H, Covic GA, et al. (2015) Investigation of Multiple Decoupled Coil Primary Pad Topologies in Lumped IPT Systems for Interoperable Electric Vehicle Charging. *IEEE T Power Electr* 30: 1937-1955.
6. Veneri O, Ferraro L, Capasso C, et al., Charging infrastructures for EV: Overview of technologies and issues. Electrical Systems for Aircraft, Railway and Ship Propulsion (ESARS), 2012. IEEE, 2012: 1-6.
7. Pantic Z, Lee K, Lukic S, Inductive power transfer by means of multiple frequencies in the magnetic link. 2013 IEEE Energy Conversion Congress and Exposition. IEEE, 2013: 2912-2919.
8. Liu N, Habetler TG, Design of an on-board charger for universal inductive charging in electric vehicles. 2015 IEEE Energy Conversion Congress and Exposition (ECCE). IEEE, 2015: 4544-4549.
9. Keeling NA, Covic GA, Boys JT (2010) A Unity-Power-Factor IPT Pickup for High-Power Applications. *IEEE T Ind Electron* 57: 744-751.
10. Pantic Z, Lukic SM (2012) Framework and Topology for Active Tuning of Parallel

Compensated Receivers in Power Transfer Systems. *IEEE T Power Electr* 27: 4503-4513.
11. Rui C, Cong Z, Zahid ZU, et al., Analysis and parameters optimization of a contactless IPT system for EV charger. 2014 IEEE Applied Power Electronics Conference and Exposition-APEC 2014. IEEE, 2014: 1654-1661.
12. Deng J, LU F, Li W, et al., ZVS double-side LCC compensated resonant inverter with magnetic integration for electric vehicle wireless charger. 2015 IEEE Applied Power Electronics Conference and Exposition (APEC). IEEE, 2015: 1131-1136.
13. Liu N, Habetler TG, Design of a universal inductive charger for electric vehicles. Transportation Electrification Conference and Expo (ITEC), 2014 IEEE. IEEE, 2014: 1-6.
14. Pantic Z, Sanzhong B, Lukic S (2011) ZCS LCC-Compensated Resonant Inverter for Inductive-Power-Transfer Application. *IEEE T Ind Electron* 58: 3500-3510.
15. Si P, Hu AP, Malpas S, et al., Switching Frequency Analysis of Dynamically Detuned ICPT Power Pick-ups. 2006 International Conference on Power System Technology. IEEE, 2006: 1-8.
16. Choi WY, Yang MK, Cho HS (2014) High-Frequency-Link Soft-Switching PWM DC-DC Converter for EV On-Board Battery Chargers. *IEEE T Power Electr* 29: 4136-4145.
17. Deng J, Li S, Hu S, et al. (2014) Design Methodology of LLC Resonant Converters for Electric Vehicle Battery Chargers. *IEEE T Veh Technol* 63: 1581-1592.
18. Pahlevaninezhad M, Drobnik J, Jain PK, et al. (2012) A Load Adaptive Control Approach for a Zero-Voltage-Switching DC/DC Converter Used for Electric Vehicles. *IEEE T Ind Electron* 59: 920-933.
19. Budhia M, Boys JT, Covic GA, et al. (2013) Development of a Single-Sided Flux Magnetic Coupler for Electric Vehicle IPT Charging Systems. *IEEE T Ind Electron* 60: 318-328.
20. Bosshard R, Kolar JW, Muhlethaler J, et al. (2015) Modeling and η-α-Pareto Optimization of Inductive Power Transfer Coils for Electric Vehicles. *Emerging and Selected Topics in Power Electronics, IEEE Journal of* 3: 50-64.
21. Zaheer A, Kacprzak D, Covic GA, A bipolar receiver pad in a lumped IPT system for electric vehicle charging applications. 2012 IEEE Energy Conversion Congress and Exposition (ECCE). IEEE, 2012: 283-290.
22. Cheng KWE, Divakar BP, Wu H, et al. (2011) Battery-Management System (BMS) and SOC Development for Electrical Vehicles. *IEEE T Veh Technol* 60: 76-88.
23. Veneri O, Capasso C, Ferraro L, et al., Performance analysis on a power architecture for EV ultra-fast charging stations. Clean Electrical Power (ICCEP), 2013 International Conference on. IEEE, 2013: 183-188.
24. Li S, Bao K, Fu X, et al. (2014) Energy Management and Control of Electric Vehicle Charging Stations. *Electr Pow Compo Sys* 42: 339-347.
25. Park SY, Miwa H, Clark BT, et al., A universal battery charging algorithm for Ni-Cd, Ni-MH, SLA, and Li-Ion for wide range voltage in portable applications. 2008 IEEE Power Electronics Specialists Conference. IEEE, 2008: 4689-4694.
26. Hõimoja H, Rufer A, Dziechciaruk G, et al., An ultrafast EV charging station demonstrator. Power Electronics, Electrical Drives, Automation and Motion (SPEEDAM), 2012 International Symposium on. IEEE, 2012: 1390-1395.
27. Vehicle Technologies Program EERE (2011) 2011 Nissan Leaf - VIN 0356, Advanced Vehicle Testing - Baseline Testing Results. U.S. Department of Energy.
28. Mishima T, Akamatsu K, Nakaoka M (2013) A High Frequency-Link Secondary-Side

Phase-Shifted Full-Range Soft-Switching PWM DC-DC Converter With ZCS Active Rectifier for EV Battery Chargers. *IEEE T Power Electr* 28: 5758-5773.
29. Aguilar C, Canales F, Arau J, et al. (1997) An integrated battery charger/discharger with power-factor correction. *IEEE T Ind Electron* 44: 597-603.
30. Du Y, Lukic S, Jacobson B, et al., Review of high power isolated bi-directional DC-DC converters for PHEV/EV DC charging infrastructure. 2011 IEEE Energy Conversion Congress and Exposition. IEEE, 2011: 553-560.